Letters

Efficient Talkative Power Conversion With Quasi-Square-Wave Zero-Voltage Switching Hysteretic Current Control

Stefan Mönch, *Member, IEEE*, Carsten Kuring, Xiaomeng Geng, Peter A. Hoeher, *Fellow, IEEE*, Marco Liserre, *Fellow, IEEE*, Rüdiger Quay, *Senior Member, IEEE*, and Sibylle Dieckerhoff, *Member, IEEE*

***Abstract*—Simultaneous power and data transmission is possible by data injection into control signals of power converters without additional hardware. In this letter, a modified analog hysteretic current control is discussed, which combines data transmission with efficient quasi-square-wave zero-voltage switching. A half-bridge GaN converter with 99.1% efficiency is investigated with respect to power conversion efficiency and data transfer. Measurements show that, compared with the digital PWM, a wider range of current ripple modulation is available for data transfer before the power efficiency drops. The feasibility of talkative power conversion (TPC) in the presence of frequency jitter is demonstrated.**

***Index Terms*—Data communication, efficiency, modulation, power conversion, power electronics, talkative power conversion (TPC).**

I. Introduction

TALKATIVE power conversion (TPC), the simultaneous transmission of power and information using a switched-mode power converter by embedding information into the switching ripple [1], [2], is possible without additional hardware effort (e.g., zero-additional-hardware power line communication (PLC) [3]). TPC is applicable both in wired systems as well as in wireless systems. Regarding wired systems, potential use cases are for example PLC replacements [4], electric vehicle battery charging [5], and battery management systems. Concerning wireless systems, TPC-based visible light communications [2], and contactless data and energy transfer systems [6], have been studied. Typically, digital control methods based on continuous conduction mode hard-switching (CCM) pulsewidth modulation (PWM), such as binary frequency shift keying (PWM/2FSK) [7] or frequency hopping-differential phase shift keying (PWM/FH-DPSK) [2], are used, with precisely known and easily detectable frequency contents. However, for the control of highly efficient power converters there exist other control methods, such as triangular current mode (TCM) [8] or quasi-square-wave zero-voltage switching (QSW-ZVS) [9], [10]. These methods have variable switching frequencies and enable ultralow switching losses (high power conversion efficiency) [11], [12] by zero-voltage switching (ZVS) [13]. The three control methods are compared in [14]. In contrast to digital control, QSW-ZVS can be achieved using an analog hysteretic current controller.

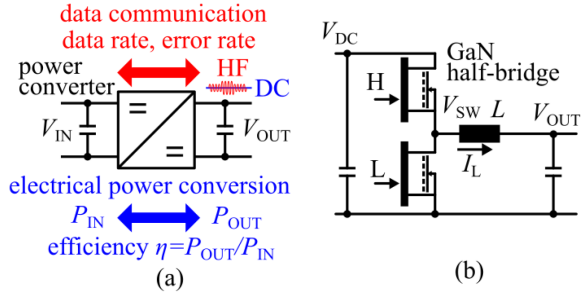

Fig. 1. (a) TPC. (b) Half-bridge converter.

This work investigates analog hysteretic current control, which enables to maintain high power conversion efficiency by maintaining low switching loss ZVS conditions over a wide range of operation points, and is especially suitable for fast-switching gallium nitride (GaN) power converters. However, such analog control introduces switching frequency jitter, which can reduce the quality of the data transmission. Experimentally, hysteretic current control of a GaN-based dc–dc converter with an efficiency of about 99% is extended by talkative data transmission using Manchester-encoded modulation of the peak current setpoint, while maintaining the valley current setpoint for ZVS. Measurements show that the talkative hysteretic current control approach maintains a high efficiency over a wider range of modulation amplitudes compared with the PWM, where ZVS is lost. Our work is applicable in all of the abovementioned applications, but is not limited to them.

The rest of this letter is organized as follows. Section II presents the proposed TPC scheme using hysteretic current control. Experimental results are reported in Section III. Finally, Section IV concludes this letter.

Manuscript received 26 May 2023; revised 7 July 2023; accepted 18 July 2023. Date of publication 20 July 2023; date of current version 1 September 2023. *(Corresponding author: Stefan Mönch.)*

Stefan Mönch and Rüdiger Quay are with the Fraunhofer Institute for Applied Solid State Physics IAF, 79108 Freiburg, Germany (e-mail: stefan.moench@iaf.fraunhofer.de; Ruediger.Quay@iaf.fraunhofer.de).

Carsten Kuring, Xiaomeng Geng, and Sibylle Dieckerhoff are with the Chair of Power Electronics, Technische Universität Berlin, 10623 Berlin, Germany (e-mail: carsten.kuring@tu-berlin.de; xiaomeng.geng@tu-berlin.de; sibylle.dieckerhoff@tu-berlin.de).

Peter A. Hoeher and Marco Liserre are with the Department of Electrical and Information Engineering, Kiel University, 24143 Kiel, Germany (e-mail: ph@tf.uni-kiel.de; ml@tf.uni-kiel.de).

Color versions of one or more figures in this article are available at https://doi.org/10.1109/TPEL.2023.3297508.

Digital Object Identifier 10.1109/TPEL.2023.3297508

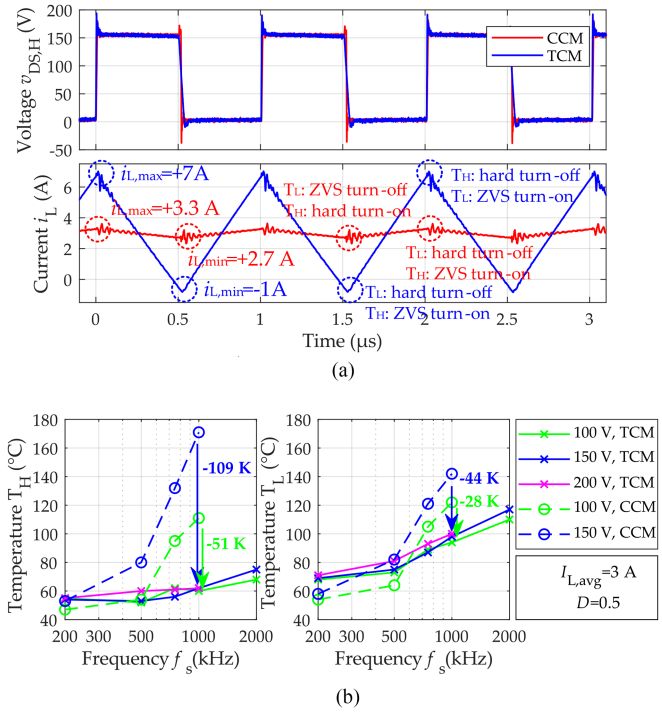

Fig. 2. GaN-based buck converter in CCM and TCM operation. (a) Transient voltage of high-side transistors and inductor current waveforms at $V_{dc} = 150$ V, $i_{L,avg} = 3$ A and $f_S = 1$ MHz. (b) Device temperature of GaN transistors T_L and T_H versus switching frequency.

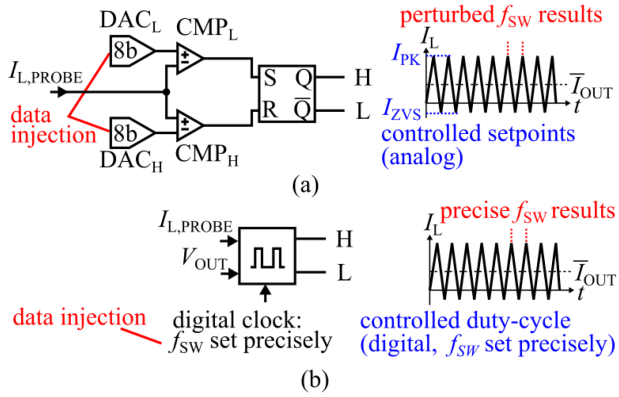

Fig. 3. Data injection. (a) Analog hysteretic current control. (b) Digital PWM.

II. Methods

A. Talkative Power Conversion

Fig. 1(a) visualizes the TPC concept [1], using a switched-mode power converter. In addition to the (dc) power conversion, an additional (software controlled) modulation of the switching signal superimposes a high-frequency signal on the output to transmit data through the power stage. Fig. 1(b) shows a GaN-based half-bridge with two power transistors (high-side H and low-side L), which is used in this work as one of the most common nonisolated power converter topologies.

Although GaN power transistors enable significantly reduced switching losses compared with the Si-based counterparts, the switching losses caused by the overlap of voltage and current increasingly dominates the power losses at higher switching frequency, thus the maximum applicable switching frequency remains limited to the low MHz-range. Fig. 2(a) shows exemplary transients of a GaN half-bridge (IGLD60R190D1S) in hard-switching CCM and soft-switching TCM at identical average load current and duty cycle. In CCM, a filter inductor $L = 64\,\mu$H is used, whereas in TCM, the filter inductor is adjusted according to $L = V_{dc}/(32 \cdot f_S)$ to achieve ZVS and maintain valley, peak, and ripple currents of -1, 7, and 8 A, respectively, at varied input voltage and switching frequency. In our setup, the output power and switching frequency are mainly limited by the device temperature of the hard-switched transistor T_H [see Fig. 2(b)]. In comparison, TCM achieving ZVS turn-ON enables a significant reduction of device temperature by up to 44 and 109 K in transistors T_L and T_H providing additional thermal headroom for even higher switching frequencies in TPC applications.

Fig. 3 compares two control methods, which can result in similar inductor current waveforms: First, Fig. 3(a) shows a hysteretic current control, where the inductor current I_L is measured by a high-bandwidth current sensor ($I_{L,PROBE}$), and then both the peak current I_{PK} and valley current I_{ZVS} are controlled by an analog comparator and flip-flop circuit. The setpoints in this work are software adjustable using two digital-analog converters. This software control of the setpoint also enables the later used modulation for data transmission. Since both current values are controlled by using an analog circuit, as shown in Fig. 3(a), the resulting switching frequency f_{SW} has jitter, resulting from noise, delays, and uncertainties from the analog signal processing stages. The hysteretic current control enables to control the valley current values, which is useful to ensure ZVS conditions in each switching cycle for a high power conversion efficiency η. The switching frequency jitter is not relevant for the power conversion efficiency. However, if this analog hysteretic current control is also used for data communication by modulation of the peak current value (while maintaining a constant valley current to ensure ZVS), it will result in frequency jitter and can deteriorate the data transmission quality. This work investigates the tradeoff between the power conversion efficiency and the amplitude of the current modulation required for data transmission.

Second, Fig. 3(b) illustrates conventional PWM, where a digital clock precisely sets the switching frequency f_{SW}, and the duty cycle is modulated. With a variable (but digitally controlled) switching frequency, PWM can also achieve ZVS conditions over a wide range of operation voltages; however, the PWM-like modulation, therefore, requires a feedback signal (e.g., the output voltage), such that the valley current is only indirectly defined (and thus not as stably controlled as with analog hysteretic control). PWM is well known for talkative power converters and regularly used for investigations focusing on the data transmission aspect of TPC. With PWM, the switching frequency is both digitally set and modulated [4], and switching frequency jitter, thus, is not an issue. However, the power conversion efficiency is affected if ZVS is lost during data transmission. While for PWM, the modulated switching frequencies result directly from the digital control; for analog hysteretic current control, the switching frequency results only indirectly from the inductor ripple (hysteresis) current and is dependent on the output voltage. It is, therefore, necessary to investigate how the concept of TPC can also be applied to the

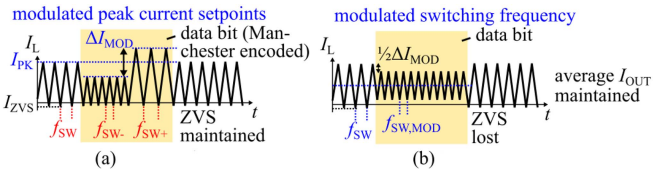

Fig. 4. Effect of modulation for data transfer on switching frequency. (a) Talkative hysteretic current control. (b) Talkative digital PWM.

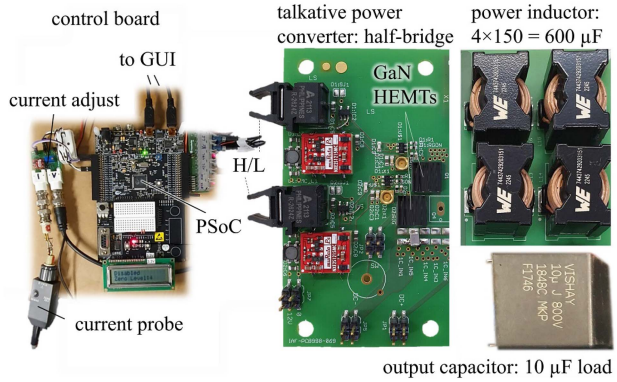

Fig. 5. Photo of the power converter setup and components used.

analog and indirect control of the switching frequencies. This work now focuses on the power conversion efficiency aspect of TPC, aiming for high efficiency using analog hysteretic current control and the resulting switching frequency jitter (possibly affecting the data transmission), which was not yet investigated.

B. Analog Hysteretic Current Control and Digital PWM

Fig. 4(a) shows how a data bit is encoded in this work by modulation of the peak current setpoints around the average peak current I_{PK}. To ensure ZVS, the valley current is kept constant. However, if only the peak current is varied, also the average output current will deviate from the intended value. To solve this issue, this work uses Manchester encoding, where the peak current is modulated by $\pm\Delta I_{\mathrm{MOD}}/2$ within one bit duration around the average I_{PK}. Within one data bit the converted power is slightly modulated, however, over one data bit a constant average output current is maintained. A rising edge "$-\Delta I_{\mathrm{MOD}}/2\ldots+\Delta I_{\mathrm{MOD}}/2$" denotes a logic "1" and a falling edge "$+\Delta I_{\mathrm{MOD}}/2\ldots-\Delta I_{\mathrm{MOD}}/2$" a logic "0." No modulation of I_{PK} is used, whereas no data ("NaN") is transmitted (normal power conversion). The modulation of the peak current directly results in a modulation of the switching frequency f_{SW}, which then causes a high-frequency voltage ripple on the output voltage (used as transmission medium).

A reduced peak current (lower hysteretic current ripple) causes a higher switching frequency $f_{\mathrm{SW}-}$ and an increased peak current a lower switching frequency $f_{\mathrm{SW}+}$ (the sign symbols refer to the change of current ripple).

In contrast, Fig. 4(b) shows a simple talkative PWM control, where a modulation between the normal switching frequency f_{SW} and a slightly modified switching frequency $f_{\mathrm{SW,MOD}}$ is used to encode a data bit. The different effects on power conversion efficiency resulting from the two modulation methods are further discussed in Section III-C. As visible in Fig. 4, schemes (a) and (b) have in common that two modulation frequencies are

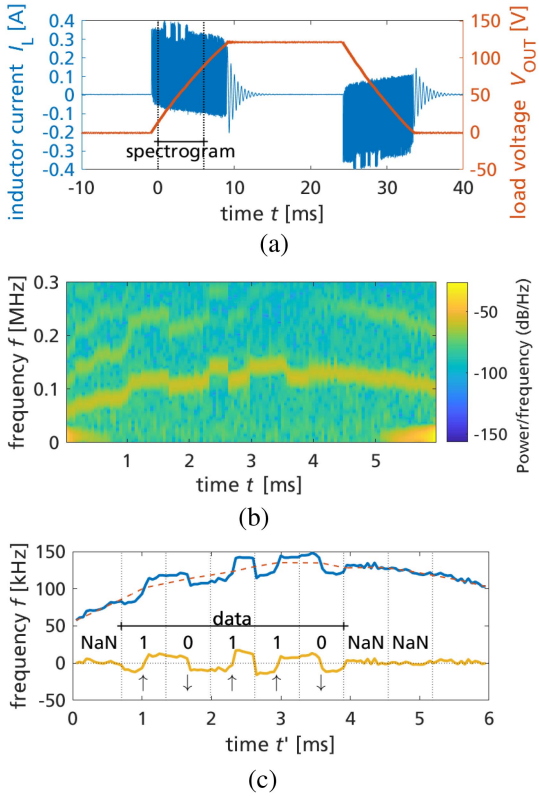

Fig. 6. Measurements: (a) Data transfer visible by peak current modulation. (b) Spectrogram of output voltage. (c) Extracted switching frequency and data.

required to differentiate data from normal converter operation. For hysteretic current control, the switching frequency f_{SW} with current ripple ΔI_{L} depends on the voltages $V_{\mathrm{IN/OUT}}$

$$f_{\mathrm{SW}}(V_{\mathrm{OUT}}) = \left(\frac{1}{V_{\mathrm{OUT}}} + \frac{1}{V_{\mathrm{IN}} - V_{\mathrm{OUT}}}\right)^{-1} (L\Delta I_{\mathrm{L}})^{-1} \quad (1)$$

$$\text{with} \quad f_{\mathrm{SW}} < V_{\mathrm{IN}}(4L\Delta I_{\mathrm{L}})^{-1} = f_{\mathrm{SW,MAX}}. \quad (2)$$

The maximum $f_{\mathrm{SW,MAX}}$ is at $V_{\mathrm{OUT}} = \frac{1}{2}V_{\mathrm{IN}}$ and f_{SW} is directly linked to ΔI_{L}. Modulation of the peak current modulates the switching frequency and is used for data transmission.

III. Results

A. Experimental Setup

A GaN-based half-bridge converter with analog hysteretic current control on a programmable system on chip is used. While Fig. 3(a) was simplified, the full implementation is found in [15], and handles special cases (start/stop and standby) and dead times. This work extends the control software by Manchester encoded data injection into the peak current setpoints (see Fig. 4) without additional hardware.

To inject one data bit D (0 or 1) into the converter, the peak current setpoint is adjusted in software during data transmission according to $I' = I + (\mathrm{XOR}(D, M) - \frac{1}{2}) \times \Delta I_{\mathrm{MOD}}$, where M is a (clock) bit continuously toggling (twice per data rate) for the Manchester encoding, and D the data bit to be transmitted (as part of a sequence of data bits to be transmitted), and I the average not modulated current setpoint (of a comparable converter without TPC-capabilities).

To demonstrate data transmission in the presence of variable output voltages with varying switching frequency according to (1), a capacitive load (10 μF) is cyclicly charged and discharged between 0 V and $V_{\mathrm{IN}} = 120$ V, covering the full (worst-case) output voltage range during data transmission. The switching frequency is expected to vary up to $f_{\mathrm{SW,MAX}} \approx 125$ kHz at nominal operation with $\Delta I_{\mathrm{L}} = 0.4$ A. The effect of load steps on data transmission should be investigated in future works, for example by using a load control bandwidth below the data modulation frequency. This work's current control can be extended by an outer voltage control as in [15].

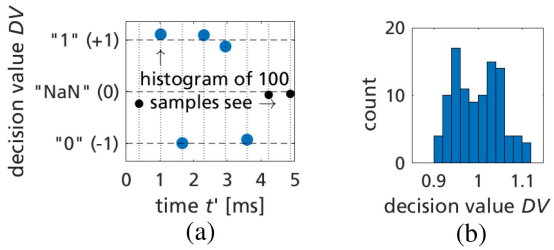

Fig. 7. (a) Decision values for five data bits. (b) Histogram for data bit "1."

B. Talkative Power Conversion and Data Decoding

Fig. 6(a) shows a representative measurement during TPC. The peak current is modulated by $\Delta I_{\mathrm{MOD}}/2 = \pm 45$ mA around the average peak current (0.35 A), resulting in expected maximum modulated switching frequencies of 112/141 kHz around the maximum nominal 125 kHz. The valley current is kept constant at -0.05 A for ZVS. A bit rate of 1.5 kHz (0.67 ms) is selected, well below the switching frequency. Increasing the switching frequency and bit rate toward the MHz-range will be part of future works and is expected to be possible using the GaN transistors [16].

Delay in the analog control loop (<100 ns) causes the actual peak and current values to be shifted in the same direction [visible as slow drift in Fig. 6(a)] depending on the output voltage. The ripple current and, thus, switching frequency are however only slightly influenced. This delay could be compensated in future by filtering the measured current signal similar to analog slope compensation for peak current control. This slow and systematic drift is an issue of the experimental setup, but does not significantly influence the data transmission. The frequency jitter, however, resulting in uncertainty between the actual and intended current setpoints, does influence the data transmission, and is further investigated.

In this work, the modulated ripple and frequency contents on the output voltage V_{OUT} (after the power inductor as a filter) are used and decoded for data transmission. The modulation, however, also causes modulated ripple and frequency contents on the input voltage V_{IN} (before the power inductor). In general, both the input and the output could be used for data transmission, with slightly different transient voltage signals (within the switching cycles) but similar modulation of the detectable frequency contents. This is because the output capacitor is charged by the continuous (triangular) inductor current, whereas the input capacitor is discharged only during one of the two switching phases of the half-bridge by a discontinuous, pulsed ramp current with offset. For channel coding and receiver design with the half-bridge circuit used in this work, the effect on output voltage is analytically calculated in [17], and a similar analysis could be carried out to analyze the effect on the input voltage. Furthermore, the data transmission method can be adapted to other types of power converters, for example to isolated, multilevel or multiphase converters, or dc–ac inverters.

The effect of data transmission on the high-frequency output voltage ripple (used for data transmission) is further analyzed using MATLAB and processing of the measured output voltage waveform: A 10 kHz high pass filter removes the dc content. Then, a spectrogram is calculated [see Fig. 6(b)]. The evaluated time region is marked in Fig. 6(a). The modulation is clearly visible. From the spectrogram, the (switching) frequency with the highest signal content ($\approx$ 50–150 kHz) is extracted and shown in Fig. 6(c) (blue trace). The average switching frequency [see Fig. 6(c), orange trace] is slowly varying because of the varying output voltage. The bit rate is known (1.5 kHz), Manchester encoding simplifies clock recovery [vertical lines in Fig. 6(c)] by introducing one edge in each bit duration even for equal consecutive data bits. The difference from the switching frequency to the average switching frequency within each bit duration is calculated (yellow trace). The edges within each bit duration are decoded as logical "0" and "1:" a falling edge is assigned to a logical "0," while a rising edge is allocated to a logical "1." In Fig. 6(c) uparrows and downarrows are shown to denote the detected edges in the middle of each data symbol. During normal converter operation, no modulation and, thus no deviation from the average switching frequency is present, indicated as "NaN." The transmitted and detected data in the example is "10110."

For data detection, a decision variable DV needs to be defined. Toward this goal, we evaluate the frequency steps in each bit duration. First, a nonnormalized DV$'$ is chosen to be the difference between the integrals of $f(t)/f_{\mathrm{AVG}}(t)$ for the first and second half of each Manchester-encoded data bit

$$\mathrm{DV}' = -\int_0^{T/2} \frac{f(t)}{f_{\mathrm{AVG}}(t)}\mathrm{d}t + \int_{T/2}^{T} \frac{f(t)}{f_{\mathrm{AVG}}(t)}\mathrm{d}t \qquad (3)$$

where $f(t)$ is the estimated frequency and $f_{\mathrm{AVG}}(t)$ the average frequency. Then, DV$'$ is normalized to become ± 1 during data transfer in the noiseless case. Fig. 7(a) depicts the normalized decision values DV for the bit sequence "10110." No data transfer ("NaN") is detected as DV ≈ 0. For data bit "1," a histogram based on 100 measurements is shown in Fig. 7(b). All decoded decision values are within 1 ± 0.1. This means zero-bit errors and scope for reducing the modulation amplitude or increasing the data rate using more sophisticated modulation and coding techniques. According to the Nyquist–Shannon theorem [7], two samples per symbol duration are sufficient to provide a set of sufficient statistics. Surely the computational effort is increased compared with the classical converters, but data transmission is provided simultaneously. The complexity is significantly less than in conventional PLC modems [3].

C. Effect of Modulation Amplitude on Power Efficiency

Higher current modulation amplitude ΔI_{MOD} simplifies data detection because of a more pronounced frequency shift. Significantly increased ΔI_{MOD}, however will operate the converter outside its intended and optimal efficiency η.

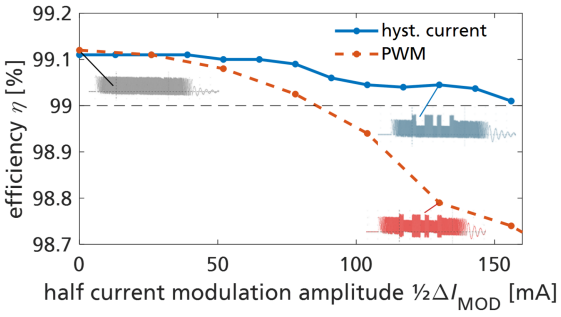

Fig. 8. Measured power conversion efficiencies.

The tradeoff between current modulation amplitude ΔI_{MOD} and power conversion efficiency η is now measured during continuous TPC. ΔI_{MOD} was stepwise increased from zero (no data) to over 300 mA. Two measurement series were conducted: one with the hysteretic current control and second where PWM was mimicked using the hysteretic current control. Therefore, the peak and the valley values were modulated. This does not resulted in precise switching frequencies as with digital PWM, but still give similar measured efficiencies as with talkative PWM.

As visible in Fig. 6(a), the average (rectified) charging power of the 10 μF load at 120 V with a system cycle time of 50 ms (20 Hz) is 9 W (during the charging/discharging bursts, without the visible standby phases), or 2.88 W (including the standby phases). The average rectified charging current is around 150 mA, whereas the total time-averaged current over a complete system cycle is zero (resulting from the bidirectional charging of a capacitive load, in contrast to resistive loads).

Fig. 8 shows efficiency measurements. At zero modulation, both control methods have similar efficiency of $\approx$99.11%, because the current waveforms are similar (gray inset). For high modulation amplitudes, PWM loses ZVS, since the valley current is not negative any more (red inset). For a negative valley current, the inductor charges the switch-node resonantly, followed by ZVS turn-ON, which is very efficient. For positive valley currents the switch-node has to be charged by a lossy hard-switching transition caused by the turn-ON of the other half-bridge transistor, which is less efficient (increased switching loss). The hysteretic current method maintains a negative valley current. PWM, however modulates both the peak and valley currents, such that for a slightly increased switching frequency ZVS is quickly lost, resulting in higher switching losses. In Fig. 4 "ZVS maintained" and "ZVS lost" is labeled. The power conversion efficiency of PWM at comparable modulation amplitudes is lower compared with the hysteretic current control (blue inset). From Fig. 8 it is concluded that both the modulation strategies enable talkative power, but the hysteretic current control, which maintains ZVS conditions, has a wider range of current modulation amplitude before the efficiency decreases. For example, using PWM the efficiency dropped to 99 % already at $\frac{1}{2}\Delta I_{\mathrm{MOD}} \approx 85$ mA, while the hysteretic current control has almost a twice as wide range up to $\frac{1}{2}\Delta I_{\mathrm{MOD}} \approx 160$ mA. This wide current range enables low bit error rates and high power conversion efficiency for the analog hysteretic current control.

The previously statistically analyzed data transmission was at a half modulation amplitude of around 50 mA. The error free data transmission was, thus, enabled by this work's analog QSW-ZVS approach with at the same time a high power conversion efficiency (insignificant drop from 99.11% to 99.1%).

IV. Conclusion

TPC can be realized without additional hardware of power converters, increasing the functionality beyond power conversion. While digital PWM is typically used for TPC, this work also shows that the analog hysteretic current control can be enhanced by data transmission, while maintaining ZVS and, thus, high energy efficiency over a wide range of modulation amplitudes.

References

[1] M. Liserre, H. Beiranvand, Y. Leng, R. Zhu, and P. A. Hoeher, "Overview of talkative power conversion technologies," *IEEE Open J. Power Electron.*, vol. 4, pp. 67–80, Jan. 2023.

[2] X. He, R. Wang, J. Wu, and W. Li, "Nature of power electronics and integration of power conversion with communication for talkative power," *Nature Commun.*, vol. 11, no. 1, pp. 1–12, 2020.

[3] R. Han and D. J. Rogers, "Zero-additional-hardware power line communication for DC-DC converters," *IEEE Trans. Power Electron.*, vol. 37, no. 11, pp. 13107–13118, Nov. 2022.

[4] W. Stefanutti, S. Saggini, P. Mattavelli, and M. Ghioni, "Power line communication in digitally controlled DC-DC converters using switching frequency modulation," *IEEE Trans. Ind. Electron.*, vol. 55, no. 4, pp. 1509–1518, Apr. 2008.

[5] C.-C. Huang, C.-L. Lin, and Y.-K. Wu, "Simultaneous wireless power/data transfer for electric vehicle charging," *IEEE Trans. Ind. Electron.*, vol. 64, no. 1, pp. 682–690, Jan. 2017.

[6] J. Noeren, J. Heinrich, M. Böttigheimer, W. Ye, and N. Parspour, "A high frequency data transmission method for contactless energy transfer systems," in *Proc. IEEE Wirel. Power Transfer Conf.*, 2018, pp. 1–4.

[7] S. S. Haykin, *Communication Systems*, 4th ed. New York, NY, USA: Wiley, 2001.

[8] U. Burkhard, "Control scheme for EMI reduction via spread spectrum modulation for triangular current mode (TCM) DC/DC converters," in *Proc. 11th Int. Conf. Integr. Power Electron. Syst.*, 2020, pp. 1–6.

[9] V. Vorperian, "Quasi-square-wave converters: Topologies and analysis," *IEEE Trans. Power Electron.*, vol. 3, no. 2, pp. 183–191, Apr. 1988.

[10] D. Maksimovic, "Design of the zero-voltage-switching quasi-square-wave resonant switch," in *Proc. IEEE Power Electron. Specialist Conf.*, 1993, pp. 323–329.

[11] D. M. Divan and G. Skibinski, "Zero-switching-loss inverters for high-power applications," *IEEE Trans. Ind. Appl.*, vol. 25, no. 4, pp. 634–643, Jul./Aug. 1989.

[12] A. Vazquez, K. Martin, M. Arias, and J. Sebastian, "Variable-width hysteretic analog control for QSW-ZVS and TCM source/sink converters," *IEEE Trans. Power Electron.*, vol. 35, no. 3, pp. 3195–3207, Mar. 2020.

[13] O. Knecht, D. Bortis, and J. W. Kolar, "Comparative evaluation of a triangular current mode (TCM) and clamp-switch TCM DC-DC boost converter," in *Proc. IEEE Energy Convers. Congr. Expo.*, 2016, pp. 1–8.

[14] A. Rodriguez, A. Vazquez, M. R. Rogina, and F. Briz, "Synchronous boost converter with high efficiency at light load using QSW-ZVS and SiC MOSFETs," *IEEE Trans. Ind. Electron.*, vol. 65, no. 1, pp. 386–393, Jan. 2018.

[15] S. Moench et al., "A GaN-based DC-DC converter with zero voltage switching and hysteretic current control for 99% efficient bidirectional charging of electrocaloric capacitive loads," in *PCIM Europe; Int. Exhib. Conf. Power Electron., Intell. Motion, Renew. Energy Energy Manage.*, 2022, pp. 1–10.

[16] X. Geng, C. Kuring, O. Hilt, M. Wolf, J. Würfl, and S. Dieckerhoff, "Study on the gate loop design and its impact on switching characteristics of GaN transistors," in *Proc. 24th Eur. Conf. Power Electron. Appl.*, 2022, pp. P.1–P.11.

[17] P. A. Hoeher, M. Mewis, and M. Liserre, "Channel coding and receiver design for simultaneous wireline information and power transfer," *IEEE Open J. Power Electron.*, vol. 2, pp. 545–558, Oct. 2021.